(Received 14 February 2024, Accepted 11 May 2024, Scheduled 15 June 2024)

Dual-Wideband MIMO Antenna with Eight Elements for 5G and WLAN Communication

Lingrong Shen[1], Jianlin Huang[1], Qiangjuan Li[1], Tian Hong Loh[2], and Gui Liu[1,*]

[1] College of Electrical and Electronic Engineering, Wenzhou University, Wenzhou, Zhejiang 325035, China
[2] National Physical Laboratory, Teddington TW11 0LW, UK

ABSTRACT: This paper presents a compact 8×8 multiple-input-multiple-output (MIMO) antenna system designed to operate across two wide frequency bands suitable for fifth-generation (5G) mobile network and wireless local area network (WLAN) applications. Each antenna element comprises a radiator, a feeding line, and a defected ground plane. Each radiator consists of a first L-shaped radiator (FLR), a second L-shaped radiator (SLR), and an extra radiator (ER). To enhance the isolation, a defected ground structure (DGS) is employed between the antenna elements. The presented antenna operates across three frequency bands, namely, 3.5 GHz (3.3 GHz–3.8 GHz) and 4.9 GHz (4.8 GHz–5 GHz) 5G frequency bands, and 5.7 GHz (5.15 GHz–5.85 GHz) WLAN frequency band, exhibiting excellent isolation, surpassing 15 dB in both lower and higher frequency bands. The overall efficiency exceeds 58%, with an envelope correlation coefficient (ECC) value below 0.125. The simulation and measurement results are in good agreement.

1. INTRODUCTION

The current era is characterized by rapid information dissemination, driving the demand for innovative antenna solutions. In recent years, fifth-generation (5G) mobile communication technology has reached a pivotal stage of development. This progress has seen the emergence of global 5G frequency bands, including N77 (3.3 GHz–4.2 GHz), N78 (3.3 GHz–3.8 GHz), and N79 (4.4 GHz–5 GHz), as well as frequency ranges allocated for IEEE 802.11a/802.11n/802.11ac at 5.15–5.35 GHz and 5.725–5.85 GHz. In response to the need for compatibility with both 5G and wireless local area network (WLAN) technologies, the integration of multiple-input-multiple-output (MIMO) technology has become essential [1]. While numerous antenna arrays have been designed for sub-6 GHz bands [2–9], the focus on antennas suitable for both 5G and WLAN frequencies has been limited, with only a few designs available [11–15].

The challenge of isolating MIMO antenna elements due to mutual coupling remains a significant issue in current research. Various methods have been explored to address this challenge. Previous studies, such as [2] and [3], did not employ specific decoupling mechanisms between antenna elements; instead, isolation was achieved through self-coupling. However, recent research has focused on developing effective decoupling techniques to enhance isolation performance. For instance, authors introduce in [4] the use of balanced mode excitation (BME) patterns to improve isolation. In another study [5], the implementation of F-shaped stubs demonstrated enhanced isolation for an ultra-wideband (UWB) MIMO antenna array. While the work presented in [6] achieved high levels of parasitic element (PE) isolation, it also highlighted compromises in overall efficiencies among the decoupling elements in the antenna systems. Moreover, the utilization of L-shaped stubs, as discussed in [7], contributed significantly to enhancing isolation within specific operational bands while meeting isolation targets. To enable dual-polarized radiation, [8] proposed four pairs of orthogonally dual-polarized loop-shaped antenna components, incorporating Pattern of Directivity (PoD) and Polarization Adjustable Device (PaD) techniques for isolation. Lastly, the design detailed in [9] features four dual-polarized square-ring slot radiators fed by pairs of microstrip-line structures to achieve improved isolation performance.

The coexistence of long term evolution (LTE) and wireless fidelity (Wi-Fi) is discussed and evaluated in [10]. Similarly, the relationship between 5G and WLAN is also homologous. In [11–13], several multiband MIMO systems are devised to realize two bands. The author utilizes an antenna element composed of an L-shaped strip, a parasitic rectangular strip, and a modified Z-shaped strip to encompass the 3.5 GHz and 4.9 GHz 5G bands [14]. An analogous structure is introduced in [16] to accomplish a dual-band 5G/WLAN antenna. By using self-decoupled antenna pairs and shorted patch antennas, [17] and [19] can counter 5G and WLAN bands, respectively. An inverted-F antenna using a novel method of decoupling is presented in [21]. Reference [22] details the design of eight L-shaped slot antennas that incorporate stepped impedance resonators. These antennas are capable of generating signals for both 5G and WLAN frequency bands.

This paper focuses on evaluating the functionality of a novel 8×8 MIMO antenna designed specifically for applications in smartphones. The proposed MIMO antenna covers the

* Corresponding author: Gui Liu (iitgliu2@gmail.com).

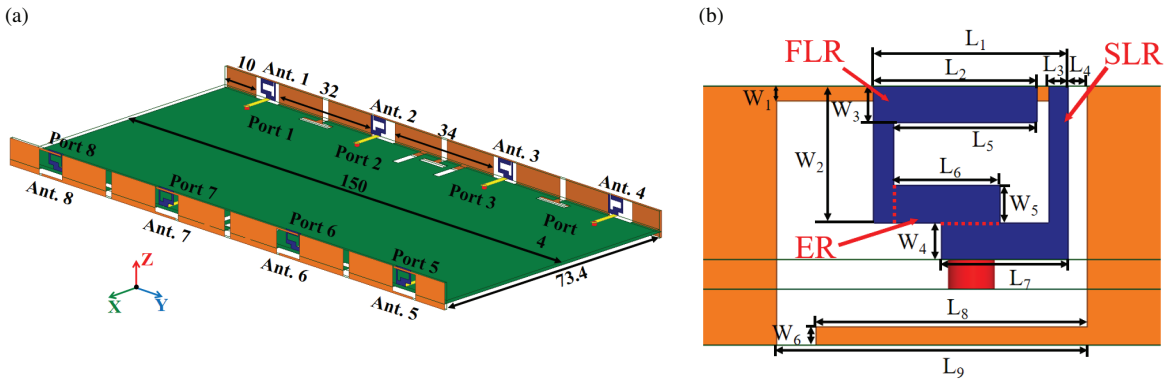

FIGURE 1. Geometry and dimensions of the proposed dual-band 8-element MIMO antenna system (Unit: mm): (a) Comprehensive Diagram, (b)Single antenna element.

3.3 GHz–3.8 GHz band (5G N77/N78 frequency bands) and 4.8 GHz–5.85 GHz band (5G N79 band and WiFi 5G band). Each antenna element consists of a radiator, a feeder line, and a defected ground plane. The isolation structure used in this paper is the defected ground structure (DGS). It is important to note that the excellent isolation in this paper does not require the addition of extra parasitic elements as in [6], but rather is accomplished by etching slots in the ground to isolate current and magnetic fields. Performance metrics such as isolation levels, envelope correlation coefficients (ECCs), and overall efficiencies are achieved across the entire working band. The proposed MIMO antenna has been fabricated and subjected to performance analysis, including an assessment over the influence of user's hands.

2. ANTENNA GEOMETRY AND DESIGN

The proposed dual-band eight-component MIMO antenna system, denoted as Ant. 1 through Ant. 8, is illustrated in Figure 1(a). The design has a length of 150 mm, a width of 75 mm, and a thickness of 7 mm, while the dimensions of the board of the antenna system are 150 mm × 73.4 mm × 0.8 mm. Two vertically mounted side frames on the sides of the system substrate have dimensions of 150 mm × 7 mm × 0.8 mm. Both the system board and two side frames are constructed using an FR-4 substrate with the dielectric constanct, $\varepsilon_r = 4.4$ and tangent loss, $\tan\delta = 0.02$. Four antenna elements are mounted on each side frame. On the reverse side of the main printed circuit board (PCB), there is a printed ground plane. Additionally, the eight radiating components are printed symmetrically and consistently on the left and right frames of this device. Each antenna element measures 8 mm × 7 mm. The detailed antenna dimensions are shown in Figure 1. The distance from Ant. 1 to the edge is 10 mm. The distances from Ant. 1 to Ant. 2 and from Ant. 2 to Ant. 3 are 32 mm and 34 mm, respectively. Since the system is symmetrical, the distances from Ant. 3 to Ant. 4, Ant. 5 to Ant. 6, and Ant. 7 to Ant. 8 are all 32 mm. The distance between Ant. 6 and Ant. 7 is 34 mm. Figure 1(b) shows the structure of an antenna element. The radiator consists of a first L-shaped radiator (FLR), a second L-shaped radiator (SLR), and an extra radiator (ER). Each radiator is connected to an external 50 Ω Sub-Miniature-A (SMA) connector via a via on the system board. In Figure 1(b), the slot sizes are indicated. The width and length of the microstrip feeding line are 1.5 mm and 8 mm, respectively. Table 1 lists all the dimensions shown in Figure 1(b) and Figure 2.

TABLE 1. The optimized antenna dimensions.

Parameter	L_1	L_2	L_3	L_4	L_5	L_6
Value (mm)	5	4.2	0.5	0.5	3.7	2.75
Parameter	L_7	L_8	L_9	W_1	W_2	W_3
Value (mm)	3.25	7	8	0.4	3.7	1
Parameter	W_4	W_5	W_6	E_1	E_2	E_3
Value (mm)	1	1	0.5	2	10	8
Parameter	E_4	F_1	F_2	F_3		
Value (mm)	12	2.4	2.8	10		

As shown in Figure 2, two types of DGS are highlighted with red dashed rectangulars. One of the most practical methods for enhancing isolation is the DGS approach, and this paper proposes T-shaped slots and ITI-shaped slots. A T-shaped slot is l positioned between Ant. 1 and Ant. 2, which effectively contributes to good isolations. The structures between Ants. 3 and 4, Ants. 5 and 6, and Ants. 7 and 8 also feature T-shaped slots. An ITI-shaped slot is located between Ant. 2 and Ant. 3, and another ITI-shaped slot is located between Ants. 6 and 7.

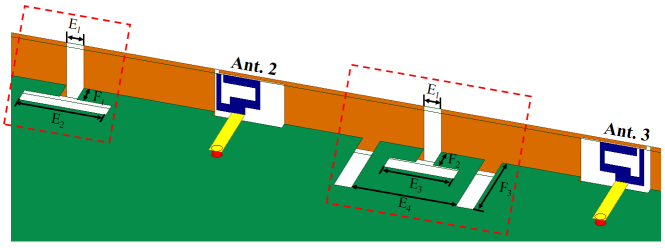

FIGURE 2. Geometry and dimensions of two defective ground structures.

The simulation results of the S-parameters of the proposed MIMO antenna system are presented in Figure 3, which are obtained by the using the commercial full wave simulator — High-Frequency Structure Simulator (HFSS). Figure 3(a) illustrates that the MIMO antenna effectively covers both

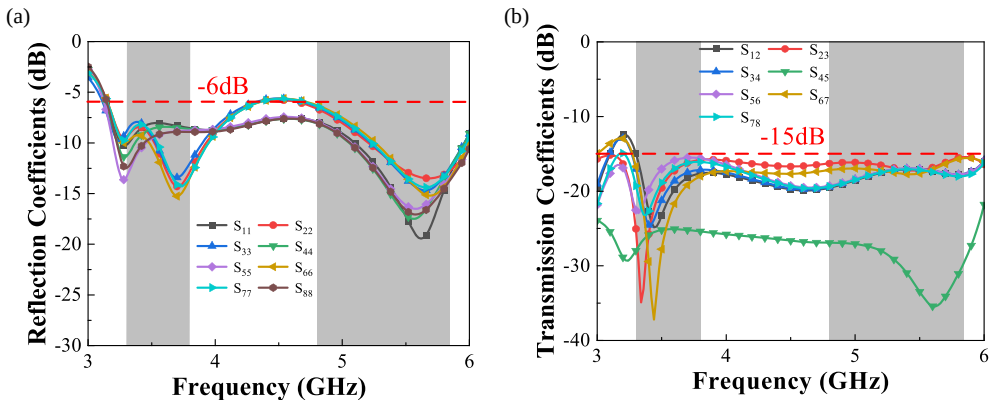

FIGURE 3. Simulated S-parameters for the proposed MIMO antenna system: (a) Reflection coefficients, (b) Transmission coefficients.

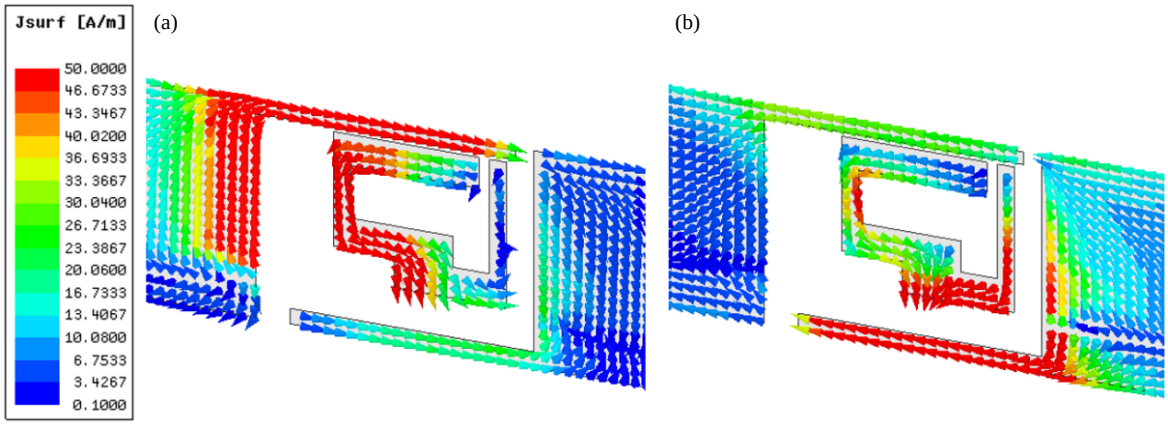

FIGURE 4. Simulated current distributions of Ant. 1 at: (a) 3.5 GHz, (b) 5.7 GHz.

the lower and upper frequency spectrum (3.3 GHz–3.8 GHz and 4.8 GHz–5.85 GHz, respectively). Furthermore, Figure 3(b) exhibits that the isolation between Ant. 1 and Ant. 2 is better than 15 dB in both the lower and higher frequency bands. Figure 3(b) reveals that the isolation values, including $S_{12}, S_{23}, S_{34}, S_{45}, S_{56}, S_{67}$, and S_{78}, consistently exceed 15 dB.

The surface current distributions at 3.5 GHz and 5.7 GHz are shown in Figure 4. At 3.5 GHz, the current is concentrated on the FLR, the ER and the left and upper strips of the outside surface . The bottom and right strips of the outside surface and the SLR and ER play the role of generating strong surface current at 5.7 GHz.

The proposed antenna must operate at dual bands in order to meet the requirements of 5G and WLAN. The evolution of the proposed antenna is depicted in Figure 5. The simulation results of the S-parameters, including the transmission coefficients (S_{12}) and reflection coefficients (S_{11}), are illustrated in Figure 6. Firstly, the rectangle patch antenna shown in Figure 5(a) operates in the 3.5 GHz frequency band. Additionally, the isolation between Ant. 1 and Ant. 2 is less than 10 dB and 15 dB in the lower and higher frequency band, respectively. Secondly, as depicted in Figure 5(b) , two slot antennas are staked on the outside of the frame, and DGSs are employed for isolation. As demonstrated in Figure 6, two bands deviate from the target bands. Finally, as shown in Figure 5(c), the proposed antenna operates at the two bands with S_{11} lower than -6 dB and S_{12} lower than -15 dB.

Figure 7 illustrates the impact of the L_6 value on both the reflection coefficients of Antenna 1 and the isolation between Antenna 1 and Antenna 2. With an L_6 value of 2.25 mm, the return loss of Antenna 1 does not meet the requirements within the specified frequency bands.Incrasing the value of L_6 to 3.25 mm results in an isolation below 15 dB in the lower frequency band. The optimal value for L_6 is determined to be 2.75 mm.

The ECC is a useful metric for illustrating the MIMO effectiveness of the proposed MIMO antenna. The simulation results of ECC and DG are presented in Figure 8. ECC is a quantitative measure that assesses the spatial correlation between two components, and is related to diversity gain. Lower the ECC values indicate greater diversity. Furthermore, a decreased ECC value is highly promising for MIMO operations. ECC can be computed using the following Equation (1)

$$\text{ECC} = \frac{\iint_{4\pi} A_{ij}(\theta,\phi)\sin(\theta)d\theta d\phi}{\sqrt{\iint_{4\pi} A_{ii}(\theta,\phi)\sin(\theta)d\theta d\phi \iint_{4\pi} A_{ij}(\theta,\phi)\sin(\theta)d\theta d\phi}} \quad (1)$$

The calculated diversity gain (DG) is related to ECC in Equation (2)

$$\text{DG} = 10 \times \sqrt{1 - |\text{ECC}|^2} \quad (2)$$

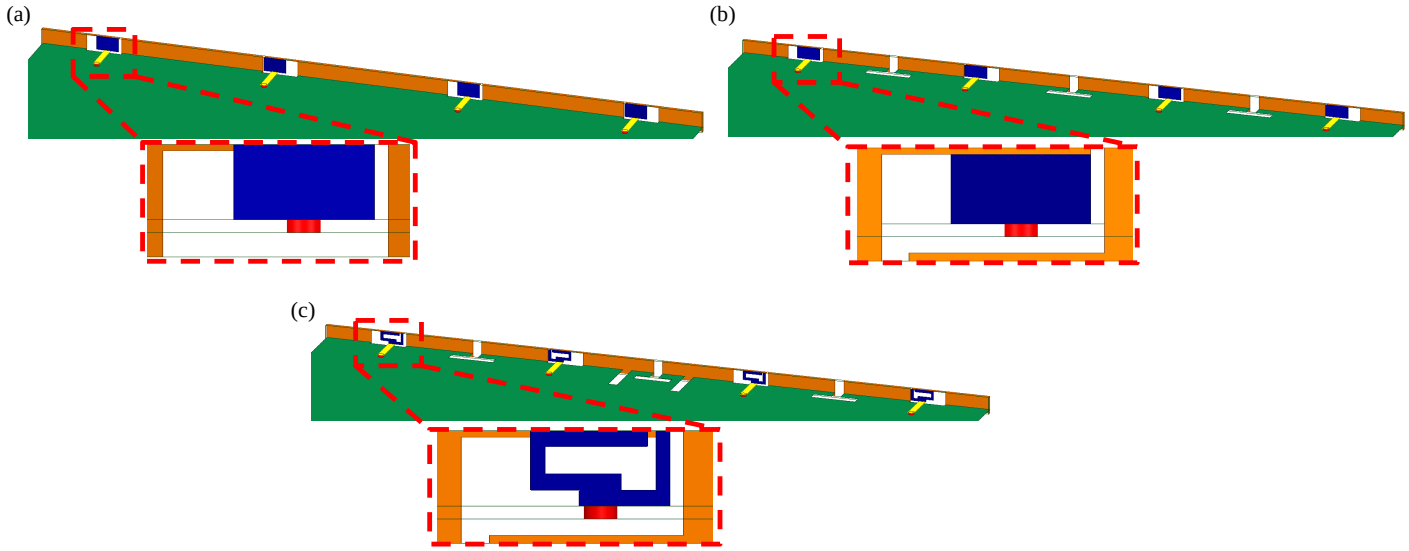

FIGURE 5. Evolutionary of the proposed antenna element in: (a) case 1, (b) case 2, (c) case 3 (our proposed design).

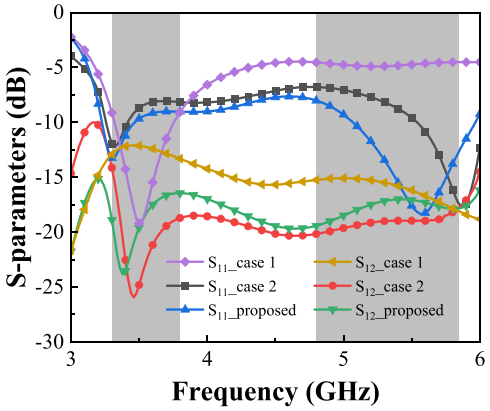

FIGURE 6. Simulacrum S-parameters for the three cases presented in Figure 5.

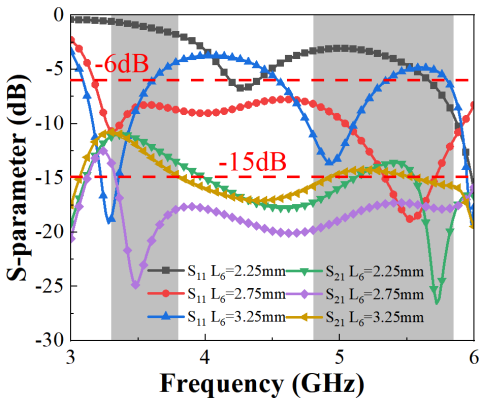

FIGURE 7. Impact of varying L_6 on S_{11} and S_{21}.

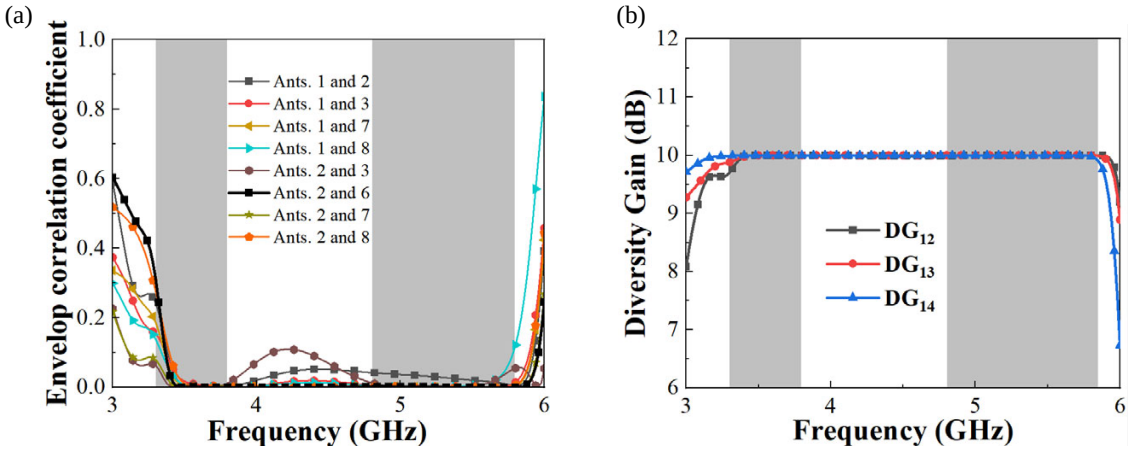

FIGURE 8. ECC and diversity gain.

The ECC serves as a crucial criterion for illustrating the MIMO effectiveness of the proposed antenna. Figure 9 shows the peak realized gain, channel capacity loss, mean effective gain (MEG) and MEG1/MEG2 of the proposed antenna. The peak realized gains are approximately 3.5 dB in 3.5 GHz band and 6.8 dB in the 5.7 GHz band, respectively. Channel capacity

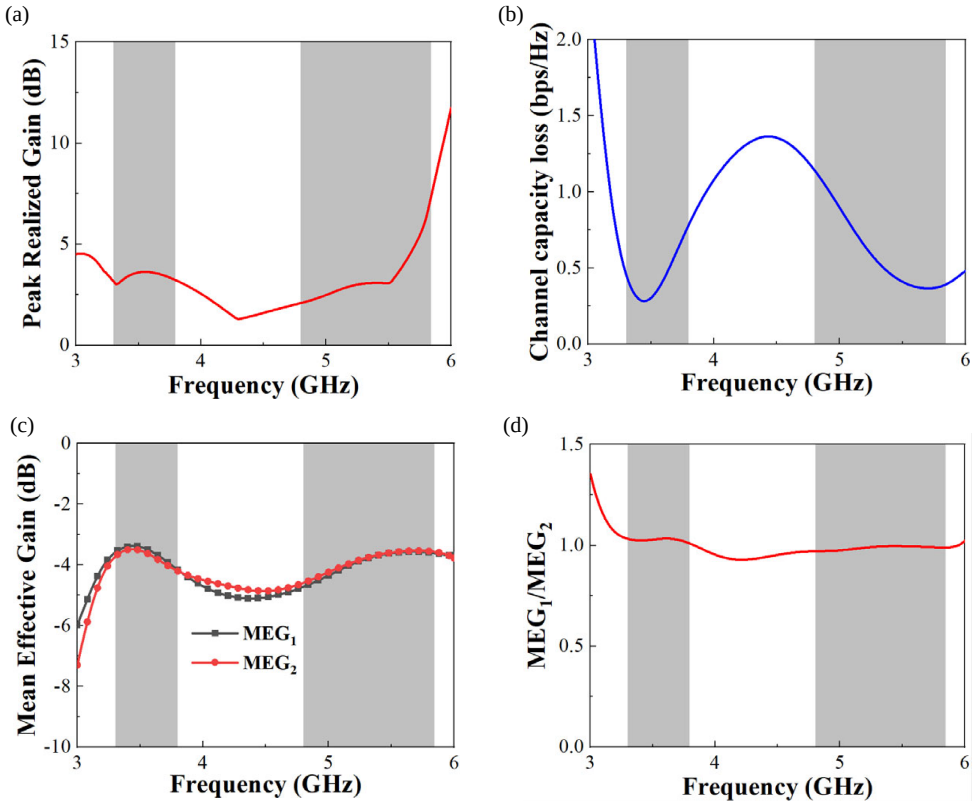

FIGURE 9. MIMO performance parameters of the proposed antenna: (a) Peak realized gain, (b) Channel capacity loss, (c) MEG, (d) MEG_1/MEG_2.

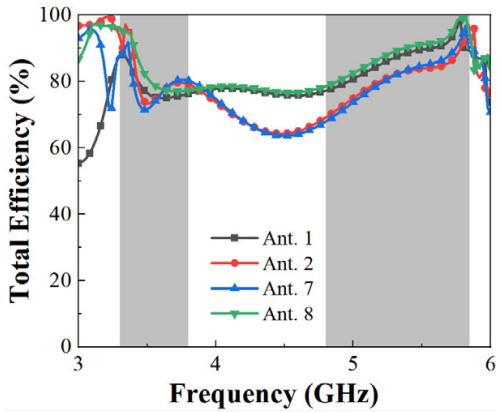

FIGURE 10. Total efficiencies of Ant. 1, Ant. 2, Ant. 7, and Ant. 8.

loss (CCL) indicates the rate of information transmitted within a communication channel without data loss. The values of CCL can be calculated by Equations (3)–(6)

$$\mathrm{CCL} = -\log_2(\psi^R) \tag{3}$$

$$\psi^R = \begin{bmatrix} \rho_{ii} & \rho_{ij} \\ \rho_{ji} & \rho_{jj} \end{bmatrix} \tag{4}$$

$$\rho_{ii} = \left(1 - |S_{ii}|^2 - |S_{ij}|^2\right) \tag{5}$$

$$\rho_{ij} = -\left(S_{ii}^* S_{ij} + S_{ji}^* S_{ij}\right) \quad \text{for } i, j = 1 \text{ or } 2 \tag{6}$$

The MEG is determined for the MIMO antenna system and is depicted in Figure 9(c) and Figure 9(d). The values of MEG_1 and MEG_2 are very close, with a difference of less than 3 dB difference. The ratio of MEG_1 and MEG_2 is close to 1, which satisfies the equality criterion for the two antenna elements.

The simulated total efficiency is depicted in Figure 10. When Ant. 1 operates independently, the total efficiencies range from 64% to 73% in the lower band and and from 72% to 84% in the higher band. When Ant. 2 operates on its own, the total efficiencies vary between 58% and 63% in the 3.5 GHz band, and between 72% to 84% in the 5.8 GHz band. Based on these findings, the feasible demand (better than 40%) for smartphones has been met.

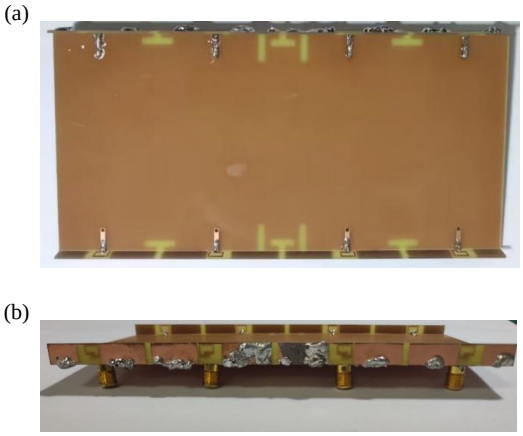

FIGURE 11. Photographs of the fabricated antenna prototype: (a) Top view, (b) Side view.

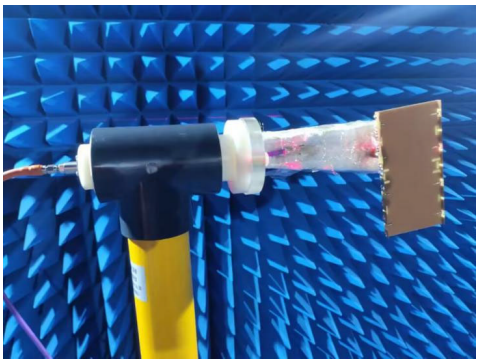

FIGURE 12. Photograph of the measurement setup in the anechoic chamber.

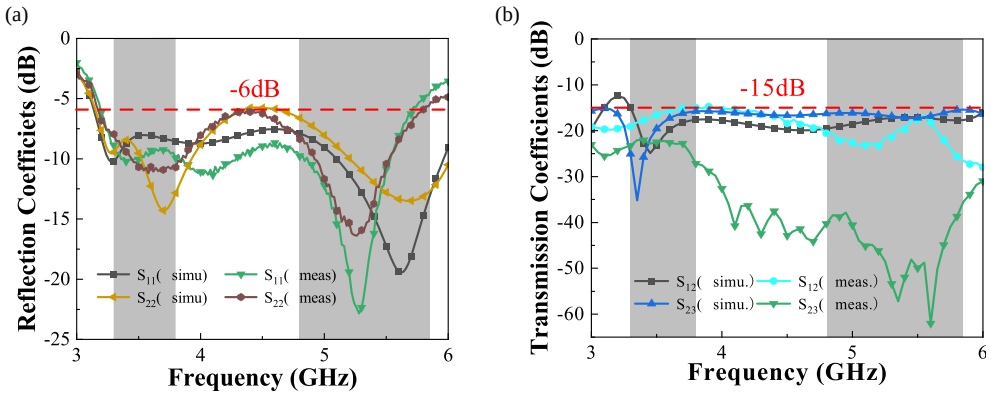

FIGURE 13. The simulated and measured S-parameters of the proposed antenna: (a) S_{ii}, (b) S_{ij}.

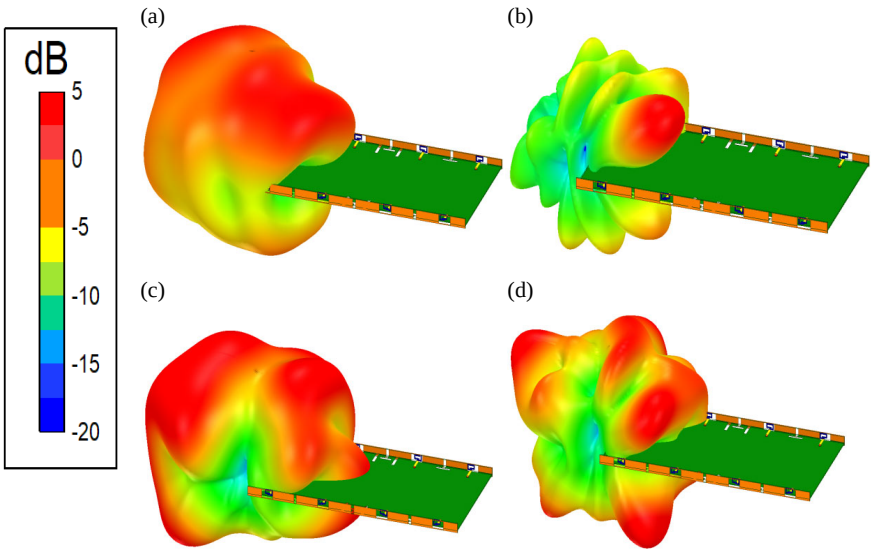

FIGURE 14. Three-dimensional radiation patterns: (a) Ant. 1 at 3.5 GHz, (b) Ant. 1 at 5.7 GHz, (c) Ant. 2 at 3.5 GHz, (d) Ant. 2 at 5.7 GHz.

3. SIMULATED AND MEASURED RESULTS

The photographs of the fabricated antenna prototype are dipicted in Figure 11, and the measurement setup in the anechoic chamber is shown in Figure 12. As depicted in Figure 11, the feeding lines are connected to 50 Ω SMA connectors through vias on the ground plane of the system board. The Keysight N5224A Vector Network Analyzer is used for measurement.

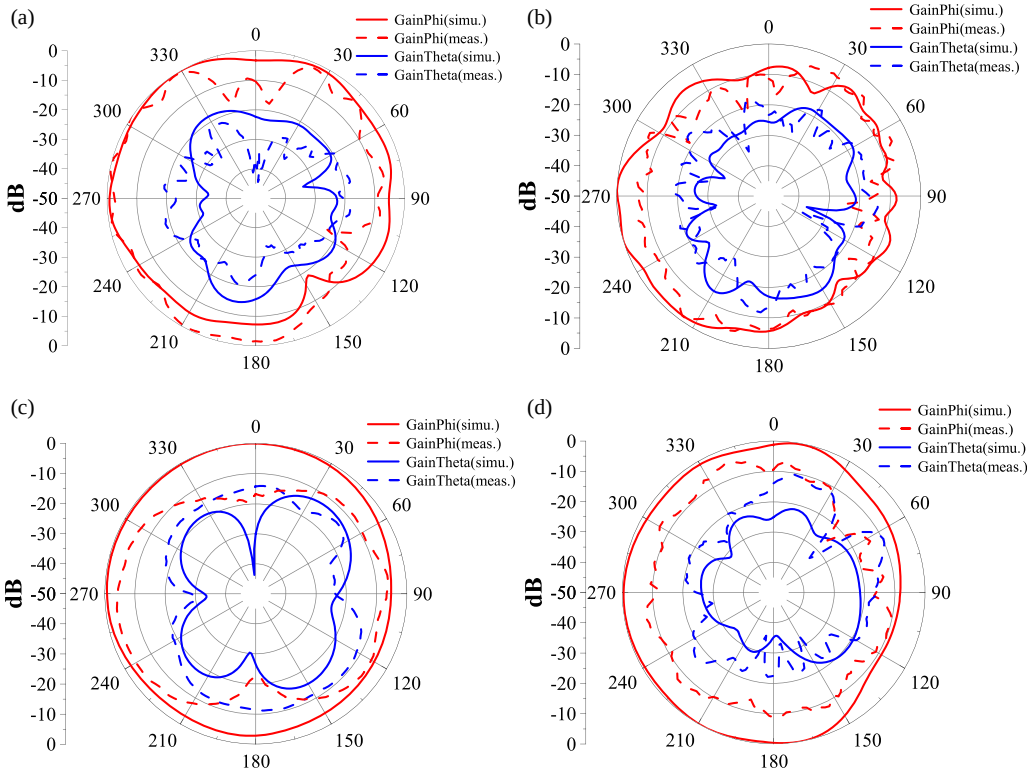

FIGURE 15. Simulated and measured normalized radiation patterns of Ant. 1: (a) 3.5 GHz at H-plane, (b) 5.7 GHz at H-plane, (c) 3.5 GHz at E-plane. (d) 5.7 GHz at E-plane.

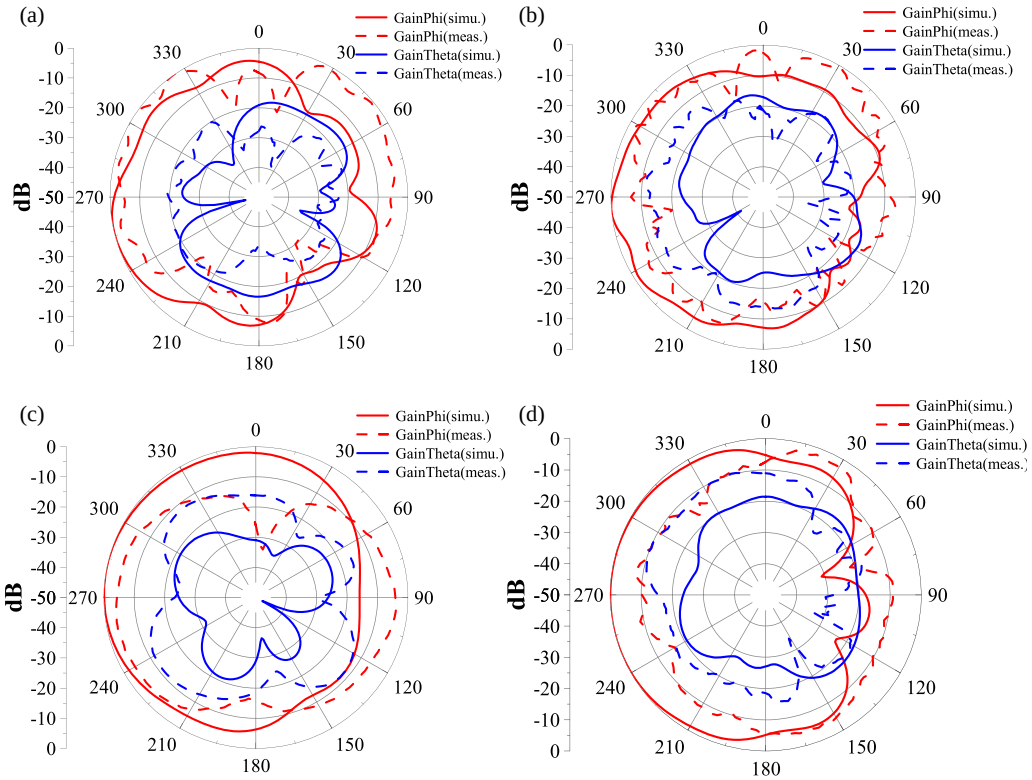

FIGURE 16. Simulated and measured normalized radiation patterns of Ant. 2: (a) 3.5 GHz at H-plane, (b) 5.7 GHz at H-plane, (c) 3.5 GHz at E-plane, (d) 5.7 GHz at E-plane.

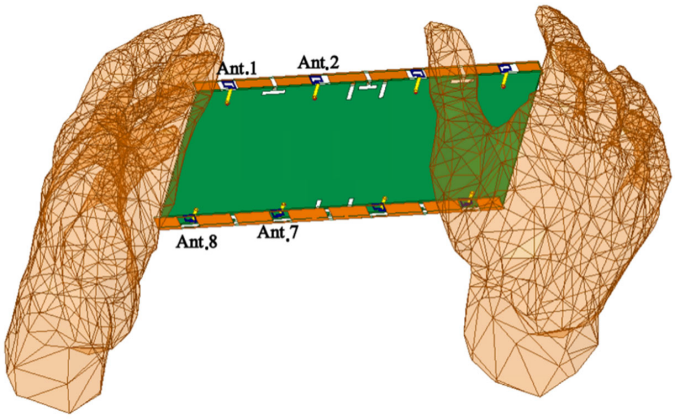

FIGURE 17. Typical configuration of the hand-grip smartphone: read mode (RM).

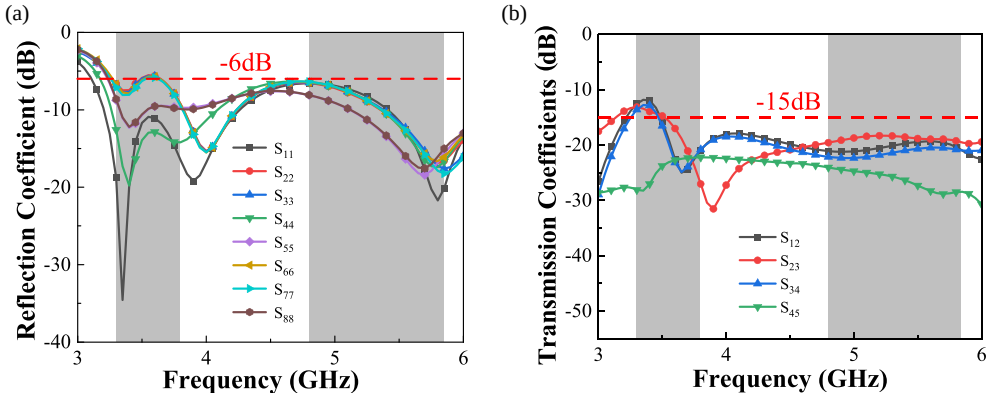

FIGURE 18. Simulated S-parameters with user hand influence on the proposed 8×8 MIMO antenna system: (a) reflection coefficients. (b) transmission coefficients.

The simulated and measured S-parameters are shown in Figure 13. The minor difference might be attributed to connection effects, manufacturing tolerances, and mesurement errors. As illustrated in Figure 13(a), the proposed MIMO antenna system has the capacity to operate within the frequency ranges of both 3.3 GHz–3.6 GHz and 4.8 GHz–5.85 GHz. In both the lower and higher frequency bands, the S_{ij} values are below -15 dB.

Figure 14 presents the simulated three-dimensional radiation patterns for Ant. 1 and Ant. 2 at 3.5 GHz and 5.7 GHz. To keep it concise, we only calculate the radiation patterns of Ant. 1 and Ant. 2 due to the symmetrical feature of the 8×8 MIMO configuration.

Figure 15 shows the normalized two-dimensional (2D) radiation patterns of Ant. 1 in both the H-plane and E-plane at 3.5 GHz and 5.7 GHz. Figure 16 shows the normalized 2D radiation patterns of Ant. 2 in both the H-plane and E-plane at 3.5 GHz and 5.7 GHz.

4. USERS' HAND EFFECTS

To simulate and study the impacts of users' hands on the performance of the proposed 8-element MIMO antenna system, ANSYS Electronics Desktop was employed. Taking the most typical scenario, the read mode (RM, dual-hands mode), as an illustration, the RM condition is depicted in Figure 17. Figure 18 illustrates the reflection coefficients and transmission coefficients of the 8×8 MIMO system. As shown in Figure 18(a), the shape and trend of the reflection coefficients of Ant. 4 are consistent with Ant. 1, as are Ant. 2 and Ant. 3, Ant. 5 and Ant. 8, and Ant. 6 and Ant. 7. These results demonstrate the symmetrical characteristics of these radiators. Antennas 1, 2, 7, and 8 exhibit the capability to provide a sufficiently wide frequency response range ($|S_{11}| > 6$ dB) that covers the 3.5 GHz and 4.9 GHz 5G frequency bands in addition to the 5.8 GHz WLAN frequency band. Meanwhile, S_{22} and S_{33} are considerably impacted by the bands in the two operational bands. Additionally, as exemplified in Figure 18(b), the proposed MIMO antenna demonstrates isolations exceeding 13 dB and 16 dB in the lower and higher frequency bands, respectively. The above results suggest that the payoff is satisfying in terms of the antennas performing well under the script of RM. Simulated total efficiency in the presence of user's hand is shown in Figure 19.

Table 2 summarizes the MIMO performance between the presented MIMO antenna and the alternate ones. When comparing the same bandwidth listed in the table with references [12–15], [18] and [20], the advantaged MIMO antenna achieves high efficiency, excellent isolation, and the lowest ECC. The primary achievement of our work is the proposal of a smaller-sized dual-band antenna element solution that offers improved MIMO antenna performance.

TABLE 2. A contrast between the proposed MIMO antenna and other references.

Reference	Operating band (GHz)	Isolation (dB)	Efficiency (%)	ECC	Size (mm^3)
[12]	LB: 3.4–3.8 (−6 dB)	> 12 (LB)	41–82 (LB)	< 0.15 (LB)	150 × 80 × 0.8
	HB: 5.15–5.925 (−6 dB)	> 12.5 (HB)	47–79 (HB)	< 0.1 (HB)	
[13]	LB: 3.4–3.8 (−6 dB)	> 11 (LB)	42–65 (LB)	< 0.15 (LB)	150 × 80 × 0.8
	HB: 5.15–5.925 (−6 dB)	> 11 (HB)	62–82 (HB)	< 0.2 (HB)	
[14]	LB: 3.4–3.6 (−6 dB)	> 17.1 (LB)	45–62 (LB)	< 0.045 (LB)	150 × 75 × 0.8
	HB: 5.725–5.875 (−6 dB)	> 34.6 (HB)	52–59 (HB)	< 0.0001 (HB)	
[15]	LB: 3.3–3.6 (−6 dB)	> 12.8 (LB)	> 71 (LB)	< 0.18 (LB)	150 × 75 × 1
	HB: 4.4–5 (−6 dB)	> 12.8 (HB)	> 68 (HB)	< 0.18 (HB)	
[18]	LB: 3.4–3.6 (−6 dB)	> 6 (LB)	> 39 (LB)	< 0.26 (LB)	63.5 × 63.5 × 0.5
	HB: 4.8–4.97 (−6 dB)	> 6 (HB)	> 42.6 (HB)	< 0.02 (HB)	
[20]	LB: 3.4–3.93 (−6 dB)	> 10 (LB)	> 50–75 (LB)	< 0.23 (LB)	150 × 75 × 0.5
	HB: 4.5–5.3 (−6 dB)	> 10 (HB)	> 50–73 (HB)	< 0.23 (HB)	
This work	LB: 3.3–3.6 (−6 dB)	> 11 (LB)	58–75 (LB)	< 0.125 (LB)	150 × 75 × 0.8
	HB: 4.8–5.85 (−6 dB)	> 14 (HB)	73–99 (HB)	< 0.1 (HB)	

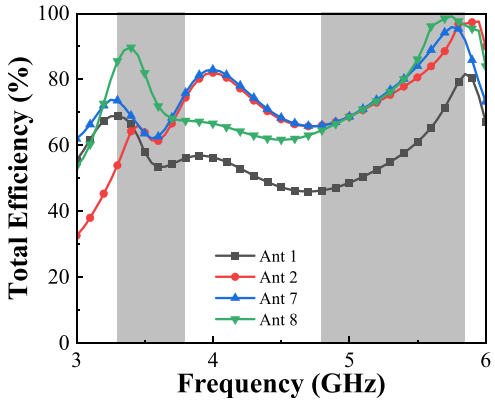

FIGURE 19. Simulated total efficiency in the presence of user's hand for the proposed 8 × 8 MIMO antenna system.

5. CONCLUSION

In this paper, we present a dual-band 8-element MIMO antenna system designed for 5G and WLAN applications within a mobile device. The system encompasses the radiating element, feeder line, and slot to achieve this purpose.The position, is crucial in producing two distinct bands. The suggested method holds great promise for the feasible implementation of multi-band MIMO technology in 5G smartmobile terminals, as it may feature a small antenna construction and superior productivity.

ACKNOWLEDGEMENT

This work was funded in part by the National Natural Science Foundation of China under Grant No. 61671330, the Science and Technology Department of Zhejiang Province under Grant No. LGG19F010009, and Wenzhou Municipal Science and Technology Program under Grant No. C20170005 and No. 2018ZG019.

REFERENCES

[1] Hong, W., "Solving the 5G mobile antenna puzzle: assessing future directions for the 5G mobile antenna paradigm shift," *IEEE Microwave Magazine*, Vol. 18, No. 7, 86–102, 2017.

[2] Deng, J.-Y., J. Yao, D.-Q. Sun, and L.-X. Guo, "Ten-element MIMO antenna for 5G terminals," *Microwave and Optical Technology Letters*, Vol. 60, No. 12, 3045–3049, 2018.

[3] Shi, H., X. Zhang, J. Li, P. Jia, J. Chen, and A. Zhang, "3.6-GHz eight-antenna MIMO array for mobile terminal applications," *AEU — International Journal of Electronics and Communications*, Vol. 95, 342–348, 2018.

[4] Yang, W. J., Y. M. Pan, and S. Y. Zheng, "Mutual coupling reduction in CP MIMO crossed-dipole antenna array," *IEEE Antennas and Wireless Propagation Letters*, Vol. 21, No. 12, 2442–2446, 2022.

[5] Iqbal, A., O. A. Saraereh, A. W. Ahmad, and S. Bashir, "Mutual coupling reduction using F-shaped stubs in UWB-MIMO antenna," *IEEE Access*, Vol. 6, 2755–2759, 2018.

[6] Li, M.-Y., Y.-L. Ban, Z.-Q. Xu, G. Wu, C.-Y.-D. Sim, K. Kang, and Z.-F. Yu, "Eight-port orthogonally dual-polarized antenna array for 5G smartphone applications," *IEEE Transactions on Antennas and Propagation*, Vol. 64, No. 9, 3820–3830, 2016.

[7] Yang, Q. C., C. Zhang, Q. Cai, T. H. Loh, and G. Liu, "A MIMO antenna with high gain and enhanced isolation for WLAN applications," *Applied Sciences*, Vol. 12, No. 5, 2279, 2022.

[8] Zhao, A. and Z. Ren, "Size reduction of self-isolated MIMO antenna system for 5G mobile phone applications," *IEEE Antennas and Wireless Propagation Letters*, Vol. 18, No. 1, 152–156, 2019.

[9] Parchin, N. O., Y. I. A. Al-Yasir, A. H. Ali, I. Elfergani, J. M. Noras, J. Rodriguez, and R. A. Abd-Alhameed, "Eight-element dual-polarized MIMO slot antenna system for 5G smartphone applications," *IEEE Access*, Vol. 7, 15 612–15 622, 2019.

[10] Xu, S., Y. Li, Y. Gao, Y. Liu, and H. Gačanin, "Opportunistic coexistence of LTE and WiFi for future 5G system: experimental performance evaluation and analysis," *IEEE Access*, Vol. 6, 8725–8741, 2017.

[11] Li, Y., C.-Y.-D. Sim, Y. Luo, and G. Yang, "12-port 5G massive MIMO antenna array in sub-6 GHz mobile handset for LTE bands 42/43/46 applications," *IEEE Access*, Vol. 6, 344–354,

2017.

[12] Li, Y., C.-Y.-D. Sim, Y. Luo, and G. Yang, "Multiband 10-antenna array for sub-6 GHz MIMO applications in 5G smartphones," *IEEE Access*, Vol. 6, 28 041–28 053, 2018.

[13] Zou, H., Y. Li, B. Xu, Y. Chen, H. Jin, G. Yang, and Y. Luo, "Dual-functional MIMO antenna array with high isolation for 5G/WLAN applications in smartphones," *IEEE Access*, Vol. 7, 167 470–167 480, 2019.

[14] Huang, J., G. Dong, J. Cai, H. Li, and G. Liu, "A quad-port dual-band MIMO antenna array for 5G smartphone applications," *Electronics*, Vol. 10, No. 5, 542, 2021.

[15] Hu, W., Q. Li, H. Wu, Z. Chen, L. Wen, W. Jiang, and S. Gao, "Dual-band antenna pair with high isolation using multiple orthogonal modes for 5G smartphones," *IEEE Transactions on Antennas and Propagation*, Vol. 71, No. 2, 1949–1954, 2023.

[16] Huang, J., G. Dong, Q. Cai, Z. Chen, L. Li, and G. Liu, "Dual-band MIMO antenna for 5G/WLAN mobile terminals," *Micromachines*, Vol. 12, No. 5, 489, 2021.

[17] Ren, Z. and A. Zhao, "Dual-band MIMO antenna with compact self-decoupled antenna pairs for 5G mobile applications," *IEEE Access*, Vol. 7, 82 288–82 296, 2019.

[18] Chen, X., J. Wang, and L. Chang, "Extremely low-profile dual-band microstrip patch antenna using electric coupling for 5G mobile terminal applications," *IEEE Transactions on Antennas and Propagation*, Vol. 71, No. 2, 1895–1900, 2023.

[19] Wong, K.-L., C.-J. Chen, and W.-Y. Li, "Integrated four low-profile shorted patch dual-band WLAN MIMO antennas for mobile device applications," *IEEE Transactions on Antennas and Propagation*, Vol. 69, No. 6, 3566–3571, 2021.

[20] Chen, Z., Y. Liu, T. Yuan, and H. Wong, "A miniaturized MIMO antenna with dual-band for 5G smartphone application," *IEEE Open Journal of Antennas and Propagation*, Vol. 4, 111–117, 2023.

[21] Zhao, X., S. P. Yeo, and L. C. Ong, "Decoupling of inverted-F antennas with high-order modes of ground plane for 5G mobile MIMO platform," *IEEE Transactions on Antennas and Propagation*, Vol. 66, No. 9, 4485–4495, 2018.

[22] Li, J., X. Zhang, Z. Wang, X. Chen, J. Chen, Y. Li, and A. Zhang, "Dual-band eight-antenna array design for MIMO applications in 5G mobile terminals," *IEEE Access*, Vol. 7, 71 636–71 644, 2019.

[23] Peng, H., R. Zhi, Q. Yang, J. Cai, Y. Wan, and G. Liu, "Design of a MIMO antenna with high gain and enhanced isolation for WLAN applications," *Electronics*, Vol. 10, No. 14, 1659–1669, 2021.